International Journal of Automotive Research, Vol. 8, No. 4, (2018), 2817-2825

Iran University of Science and Technology

International Journal of Automotive Engineering

Journal Homepage: ijae.iust.ac.ir

ISSN: 2008-9899

Admission Effects on the Flow Behaviour of a Double Entry Turbocharger Turbine

Mohammad Hasan Shojaee fard[1], Azadeh Sajedin[2] Abolfazl Khalkhali[2*],

[1] Mechanical Engineering Department, Iran University of Science and Technology, Tehran, Iran
[2]Automotive Simulation and Optimal Research Laboratory, School of Automotive Engineering, Iran University of Science and Technology, Tehran, Iran

ARTICLE INFO

Article history:

Received: 18 Mar 2018
Accepted: 29 Nov 2018
Published: 01 Dec 2018

Keywords:

Dual entry turbine
Partial admission
Unequal admission
Secondary flow
vortex

A B S T R A C T

Dual turbocharger turbine is fed by an unequal out-of-phase mass flow charge almost all the time which have significant effects on its performance parameters and flow phenomena which are not well known. Besides fully understanding the flow behavior in the radial turbine suffers from lack of detailed information about the secondary flows. This article studies the secondary flow structure within a dual entry turbine in different admission conditions. Results showed that with increasing the inequality of pressure ratio in the entries, performance of the turbine significantly decrease. From the results a profoundly disturbed flow in the interspace region was recognized. The pressure distribution of each limb shows some dependency between entries. To fully understand the flow physics, the 3D computational fluid dynamics (CFD) was implemented and compared with the experimental results of Copeland et al. (2010). The results are used to study the physical origin and the effect of nonuniform mass flow on secondary vortices. The generation and the development of the inflow, horseshoe and the corner vortex was investigated by evaluating contour plot of velocity distribution. Results demonstrated that the inflow vortex is due to the asymmetrical flow into the passage from the volute.

1. Introduction

Double entry turbines are becoming increasingly popular with automotive engine manufacturers. It has two benefits: firstly, exhaust pulse overlap decreases. Secondly, more of the pulsating exhaust flow energy will preserve [1]. The addition of a second inlet to the volute introduce extra complexity in defining the turbine performance.

Studying the performance of the turbine in unequal admission can be beneficial to match the turbine with an engine. The matching process based on the steady-state maps [2]. In unequal admission case which is the real condition, an unavoidable out-of-phase air flow is forced by the engine firing order and separated groups of cylinders. So it is much more complicated to be calculated than equal feeding. Equal admission condition is like a single entry feeding. In the partial admission situation one of the entries is empty of charge [3].

Several studies have been published over the years regarding the effects of unequal admission effects on turbine performance. Copeland et al. [4–6] and Copeland [7] performed detailed tests on a double volute turbine. They found a significant efficiency penalty when the flow inequality increases across the two entries, especially at the lower powers. Copeland [6, 7] found some dependency among the limbs even when they were kept entirely separate. Their results found with constant pressure ratio across one of the limbs, the pressure ratio of the other limb reduces, the mass flow through the fixed pressure limb was found to increase. Conversely, pressure ratio rise in the one entry leads to reduce the mass flow through the unchanged pressure side. The results showed how the high-pressure entry flow would over-

* **Abolfazl Khalkhali**
Email Address: ab_khalkhali@iust.ac.ir
10.22068/ijae.8.4.2817

[DOI: 10.22068/ijae.8.4.2817]

expand into this region efficiently throttling the flow from the other entry with the low-pressure fluid. Also, considerable dissipation will happen in this area due to mixing the higher velocity flow from one limb and the lower velocity flow from the other one. Newton et al. [8] focused on the entropy in a partial admission double entry turbine. They realize that the entropy generation in the nonflowing section of the rotor wheel has the same magnitude as that in the working part. Also, they showed when the vortices in the nonflowing area enter to the flowing part of the volute; further losses will generate. Romagnoli et al. [9] suggested a method for predicting the unequal admission mass flow for double and twin turbine from the full admission maps in different feeding. In this research, they concluded that the double entry turbine performance prediction is more difficult than twin one. When the primary objective is efficiency and total pressure ratio gain, secondary flow should be defined and controlled [10]. Secondary flow regions are always the origin of higher losses. Cascade passage, corner, tip clearance and horseshoe vortex also annulus end wall boundary-layer are some well-known vortex structure in axial turbines. They are not independent mechanisms. As can be observed in experiments they overlap and interact [11].

The secondary flow characteristic, for a given blade geometry, is influenced by the blade loading, by the load distribution, by the incidence and by the inlet boundary layer. In the last decades, most studies investigated these parameters for different airfoils, and today it is commonly believed that the classic secondary flow patterns in linear cascades are adequately understood [10].

Knowledge of physical origin of the correlated "secondary loss" and upstream nonuniform flow effects on the generation of secondary flows and relative losses on the following passages is not complete. The laminar or turbulent nature of the inlet boundary layer influences the structure of the secondary vortices, the endwall, and the mixing losses [12].

As mentioned there have been many publications describing the structure of the secondary flow in axial cascades. Ghorbanian et al. [13] investigated the vortices in an axial compressor. They figured out that the multi-blade cascade geometry, the adverse pressure gradient, and the reduction in mass flow rate which increases of the inlet angle of attack in a constant rotating speed affect the vortices generation in this case. There are only a few published studies on the construction of secondary vortices in a radial turbine cascade. Moving, growing and the diffusion of an instability vortex in the cascade flow are completely different from those of a separated vortex on an airfoil with a high angle of attack [14]. Mohammad Putra et al. [15] studied the secondary flows in a radial one entry scroll turbine nozzle. They showed that the passage vortex of the axial turbines is not found in radial turbines, instead, another single vortex can be observed, which called the "inflow" vortex. However, they studied a one entry scroll turbine which feeds the turbine by a relative uniform entrance air flow. The investigated issue in previous work on dual scroll radial turbines was the performance prediction. It is the first try to study the secondary flow physics in dual turbocharger turbine under partial and unequal admission condition. In this paper, a 3D computational analysis of the flow through a double entry turbine under different admission cases is presented. The computational results are validated by experimental data produced by the turbocharger laboratory at Imperial College London [7].

The validated model was applied to study in detail the origin and formation of the different vortex in passages and the flow structure. The presented study is a very beneficial way to study inflow vortex because every passage has a different internal mass flow.

2. COMPUTATIONAL ANALYSIS

The analyses were run by Ansys CFX 16. The transport equations were discretized with applying finite volume method. Logarithmic wall function was used to obtain the near-wall velocities. The advection terms were defined by a second-order discretization scheme; the standard k-ϵ turbulence model was used to model the turbulence. In a turbine with dual volute, the flow around the rotor is introduced nonuniform so the acceptable result only can be obtained by taking into account all the circumference instead of using periodicity and modeling one passage.

[DOI: 10.22068/ijae.8.4.2817]

In unequal admission cases a fully transient solution is required. A frozen rotor interface between domains to capture the relative motion of the stator and rotor was used as the interface in equal admission but for unequal admission a "Transient Rotor Stator" was implemented.

The sensitivity analysis in figure 3 depicts the results was depended to mesh size even with 4 million elements, after 2.5 million mesh no noticeable effect was seen. So the final mesh density selection was chosen as a balance between precision and computational expenditure. In this analyses, the second Mesh was selected, which contained 2638512 elements (figure 3).

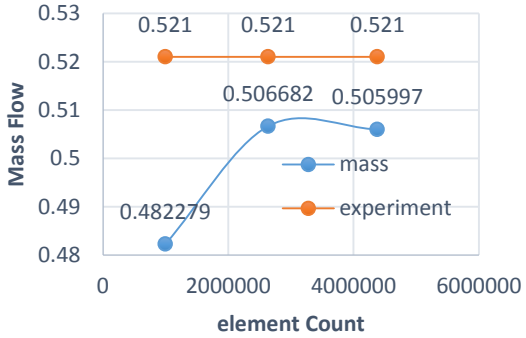

Figure 1. Mesh sensitivity analysis of whole turbine Both the full and the partial admission analysis used the same mesh.

The convergence of a solution can be judged by the residual values in iteration steps. The residual value is calculated for each finite volume within the flow domain and normalized as a function of the flow through each. For convergence of the analyses the minimum RMS residual convergence set to 1×10-5, this is an acceptable convergence by CFX [17] in some cases the convergence reached to 1×10-7.

Also, to be sure that all flow structures were accurately captured, contour plots at different stream-wise distances were produced. The mesh size was raised until the region size filled by the flow feature did not change.

1.1 Performance Parameters

In the case of equal admission, pressure ratios, mass parameter, and velocity ratio, are identical to a single entry turbine. Once the flow conditions between the entries differ, these values must be re-evaluated to account for each flow appropriately. Definition an inlet pressure that is representative of the entire turbine to obtain an overall pressure ratio and a mass parameter which could be like the single entry case is controversial. Pischinger and Wunsche [16] showed their results using averaged pressure ratio. While in a double-entry turbine, two half of the turbine wheel experience a different pressure, so using a mean inlet pressure, does not seem meaningful or appropriate. Therefore, it only seems suitable to treat the two entries separately and calculate independent pressure and mass flow parameters as follows [4]:

$$PR_{inner} = \frac{(P_{01})_{inner}}{P_4} \qquad PR_{outer} = \frac{(P_{01})_{outer}}{P_4}$$

$$MP_{outer} = \left(\frac{\dot{m}\sqrt{T_{01}}}{P_{01}}\right)_{outer} \qquad MP_{inner} = \left(\frac{\dot{m}\sqrt{T_{01}}}{P_{01}}\right)_{inner}$$

Calculating the turbine stage efficiency is easy because the total isentropic energy in each entry can be simply summed.

$$\eta_{t-s,total} = \frac{\dot{W}_{actual}}{\dot{W}_{is.inner} + \dot{W}_{is.outer}} \quad (3)$$

Lastly, Equation (4) provides the definition for the overall velocity ratio under equal or unequal admission.

$$\frac{U_2}{C_{is}} = \frac{\pi \cdot d_2 N}{\sqrt{2.\left(\frac{\dot{W}_{is.inner} + \dot{W}_{is.outer}}{\dot{m}_{total}}\right)}} \quad (4)$$

Two further parameters, useful for the following analysis, are the mass flow ratio and the effective area. The mass flow ratio defines the degree of unequal admission from 1 in full admission to 0 in partial admission [9]

$$MFR = \frac{\dot{m}_{LP}}{\dot{m}_{HP}} \quad (5)$$

Where $\dot{m}_{LP}$ represents the mass flow rate of the lower pressure limb and $\dot{m}_{HP}$ is the mass flow of the high-pressure limb. The parameter (1-MFR) used in the following analysis which bounds from 0 in equal feeding, to 1 in partial admission. The effective area is specified by the throat area of an isentropic nozzle such that, for a given expansion ratio, its mass flow will match that of the turbine. This parameter expresses the swallowing capacity of a turbine; its use in turbochargers is particularly relevant as for many simple 1D engine modeling codes it is often easier to treat the turbine as a simple nozzle [4].

$$A_{eff\,inner} = \frac{\dot{m}_{inner}}{\rho^*_{is\,inner} C^*_{is\,inner}} \quad (6)$$

[DOI: 10.22068/ijae.8.4.2817]

$$A_{\text{eff inner}} = \frac{\dot{m}_{\text{outer}}}{\rho^*_{\text{is outer}} C^*_{\text{is outer}}} \quad (7)$$

Although the effective area can be assumed as a constant, it is to some extent dependent to the rotational speed and the expansion ratio.

1.2 Geometry and Boundary Conditions

Steady-state CFD analyses were performed for the radial inflow turbine turbocharger figure 1.

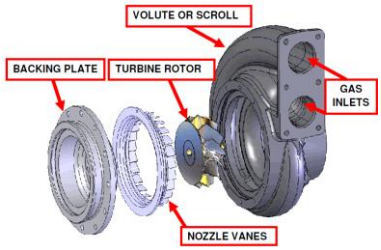

Figure 2. Geometry of main components of turbocharger turbine [5]

The major components were modeled. The generalized Grid Interface (GGI) and the frozen rotor interface boundary condition are the two interfaces which are used to coupling the grids of the scroll, stator, rotor, and exhaust channel. Figure 2 shows the rotor mesh.

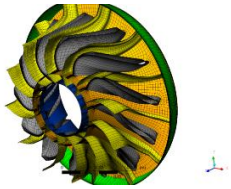

Figure 3. Rotor mesh

The boundary conditions which were Total pressure and temperature at the entrance and static pressure at the exit were defined by experimental data in two categories, five operational points for equal admission and four cases for simulating unequal admission.

Four cases were selected to be modeled:

1. Case 1: (1-MFR=0.1)
2. Case 2: (1-MFR=0.4)
3. Case 3: (1-MFR=0.6)
4. Partial admission: (1-MFR=1)

1.3 Comparison with Experimental Data

Validation of full admission results in turbine models could be investigated by major performance parameters which are used to specify the performance map.

$$MP_o = \left(\frac{\dot{m}\sqrt{T_{01}}}{P_{01}}\right)_0$$

$$PR_{Ts} = \frac{(P_{\text{total}})_{01}}{P_{\text{static exit}}}$$

$$\frac{U_3}{C_{is}} = \left[\frac{N}{\sqrt{T_0}}\right] \cdot \frac{\pi \cdot d_2}{\sqrt{2.C_p.\left(1 - \left({}^{P_4}/_{P_{01}}\right)^{\frac{\gamma-1}{\gamma}}\right.}}$$

$$\eta_{t-s} = \frac{\tau\omega}{\dot{m}C_pT_{01}\left(1 - \left({}^{P_5}/_{P_{01}}\right)^{(\gamma-1)/\gamma}\right.}$$

Figures 4 and 5 present two plots of turbine performance map in full admission case. The computational results were validated by the equal admission mass parameter and efficiency measured by Copeland (2009).

The boundary condition of five modeled points was taken from the test data. Figure 4 demonstrates the flow characteristics by plotting relative mass parameter versus total-to-static pressure ratio and figure 5 shows the relative turbine efficiency characteristics by plotting total-to-static relative efficiency against velocity ratio.

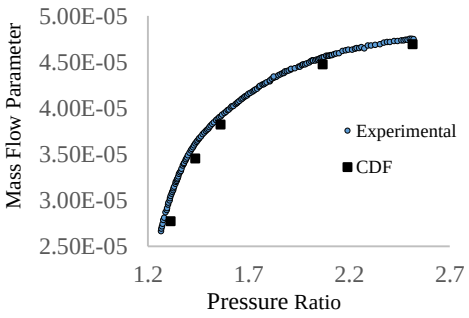

Figure 4. Comparison of computed and measured Pressure Ratio against Mass Flow Rate

Pressure ratio ranged between 1.3 and 2.5 which equated to velocity ratios between 1.12 and 0.6 respectively.

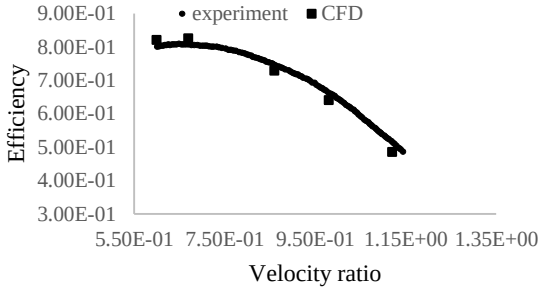

Figure 5. Comparison of computed and measured efficiency against Velocity Ratio

Below an isentropic velocity ratio of around 0.75, the computational analysis over predicts the efficiency than the experimental measurements. While at velocity ratios more

[DOI: 10.22068/ijae.8.4.2817]

than 0.75 the CFD model predicts the calculated efficiency about 9 percent lower. Maximum discrepancies are seen in the lower efficiencies of the turbine performance line; this is the area of the most enormous uncertainty in the experimental results(Copeland 2009). With the purpose of validation of unequal admission in dual turbines, a parameter related to mass flow is required. Here the effective area was used to present the performance of the dual entry turbine in unequal admission cases which is a standard parameter in this field. Using this parameter is stand from treating each turbine entry as a nozzle with a varying area A_{is} as in figure 6.

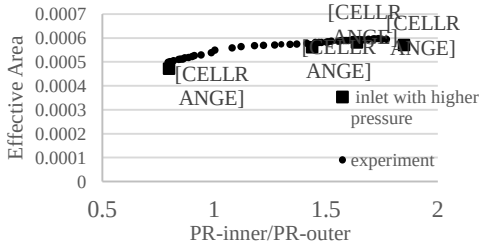

Figure 6. Effective area variation versus pressure ratio

The effective area represents the area of an ideal nozzle that is required to produce the mass flow and isentropic velocity calculated from the pressure ratio measured across each entry [4].

$$A_{is}=\frac{\dot{m}}{\rho_s \times C_{is}} \qquad (12)$$

A large variety of flow area due to a varying pressure ratio is represented in figure 6 for the turbine entries. The effective area is calculated under various degrees of admission for upper entry. Like the equal admission results, the CFD simulation seems to model the mass flow characteristics well.

3. RESULT AND DISCUSSION

With increasing the flow inequality between two limbs the efficiency decreases. Figure 7 shows the efficiency of the turbine in partial admission condition. The velocity ratio referred here is the average velocity ratio as calculated by Eq. (4). In the extreme, when the flow is only fed in one entry, the volute becomes mismatched with the rotor, and at any instant in time, only half of the rotor experiences mass flow. In this manner, the double entry turbine works in wind-mill mode. Some of the useful power provided in the flowing section of the rotor is used by the other one, and it produces positive work. Dissipated work generate entropy, so an overall decrease in the isentropic efficiency of the turbine can be observed. Also as the inequality increase the incidence angle increase therefore separation region grow on the blade surface. As a rule, As bigger the separation zone is, the pressure loss is greater and the efficiency is lower[18].

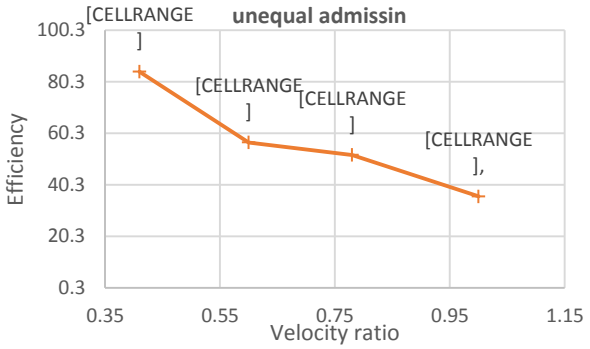

Figure 7. Drop of efficiency with increasing inequality

In partial admission case, the above entry has the equal pressure with full admission, but the lower entry is modeled with wall condition. What is expected is that the sector which experiences the flow have the same behavior like the full admission and the other 180 degrees of the rotor which receive no charge does not make any expansion. However, what is seen is different (figure 8).

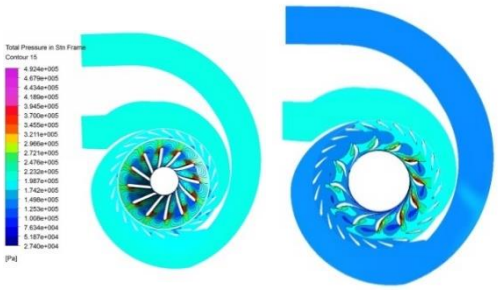

(a)Equal admission (b)Parialadmission

Figure 8. Pressure distribution in different admission

Firstly the leading edge pressure of blades that are exposed to mass flow does not experience the same pressure amplitude. The maximum pressure of the blades with the highest pressure decreased. The level of pressure on leading edges related to empty entry is higher than the expected value. This shows some dependency of entries to each other and adjust the peer researcher's findings [5]. It is concluded that some mixing of inlet flow happened before the rotor. With more investigation of figure 8, a different order of pressure can be recognized in the interspace region. So the effect of entries to

[DOI: 10.22068/ijae.8.4.2817]

each other start from the trailing edge of the stator blade.

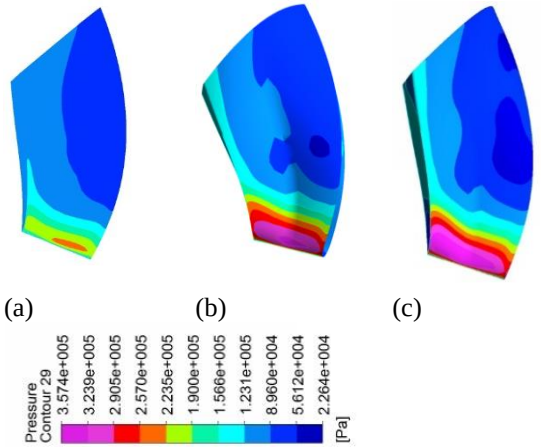

Figure 9. Pressure distribution in different admission,(a)Partial (1-MFR)= 1, (b)C3: (1-MFR)=0.6, (c)C1: (1-MFR)=0.1

The pressure distribution on rotor blades in figure 9 shows that as the (1-MFR) decreases, the contour of lower pressure level grows on the trailing edges. In other words expansion ratio increase with closing to the equal admission.

1.4 Flow Physics Under Unequal Admission

Figure 10 shows that how the inequality affects the flow in the interspace region between the nozzle blades and the rotor. The figure shows how the gas from the high-pressure limb passes its related blade and develop to the other passages. The high-pressure flow, throttle the flow from the low-pressure limb. The interspace region with significant mixing, leading to high dissipation and a considerable amount of losses in partial admission (figure10, region b). This adjusts the findings of Newton and Romagnoli [19].

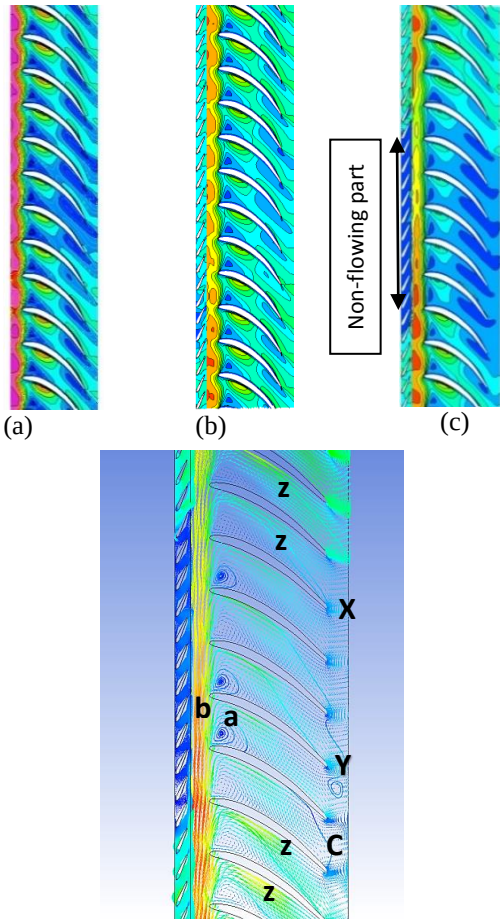

Figure 10. Velocity distribution vectors in different admission, (a)Unequal case 1, (b)Unequal Case 2 , (c)Partial admission

Figure 11 depicts the transitional character of the velocity field in the rotor. Iso-contours changed in a circumferential direction near the trailing edge which indicated a cross-pressure gradient. This pressure gradients induces a secondary flow (figure 11(c)).

- Inflow, Corner and Horseshoe vortex are the main vortexes between blades. The contour of Mach number measured from the sectional direction at the 50% span can be observed in figure 11. The Mach number spans from 0.02 to 1.2. According to Binder and Romey [20], vortexes are apparent from this plot.

Corner vortex:

The corner vortices are formed between the blade trailing edge and the end wall. Vortices generation is the results of the transportation of low energetic material (figure 10, region y). The absence of cross-pressure gradient which induces secondary flow leads to stay attached up to the blade surface and showing no

[DOI: 10.22068/ijae.8.4.2817]

deflection to the adjacent vane(figure 10, region x). The corner vortices are not identical with each other in the aspect of form and strength. These differences are due to the interaction with the inflow vortex, which plays a very dominant role at the blade exit (figure 10). After leaving the trailing edge, the corner vortices are recognizable yet (Figure 10). The accumulation of low energetic fluid (low velocity) is visible in the corner of end walls and the wake (figure10, region c).

The corner vortices are significantly weaker in flowing section than the nonflowing section. The centers of the vortices move slightly toward midstream and contribute in passage vortex meanwhile growing in this direction. In the passages with entering charge, the corner vortices tend to attach to the blade trailing edge. Inversely in passages related to empty limb vortices from the trailing edge deflect to the suction side (figure 11, red ovals).

Horseshoe vortex:

When the incoming flow encounter the stagnation point of the blade the horseshoe vortex is produced. Figure 11 shows the horseshoe vortices in the passages. Inside the vortex (B) on blades 1 and 12, the flow reaches to the transonic condition; the minimum Mach number is Ma= 0.02.

The horseshoe leg of the pressure side in flowing passage looks significantly stronger than the empty one (figure12 (b)). These differences are because of the asymmetrical and different incoming mass flow from the scroll. The weakening process of the pressure side leg of the horseshoe vortices during the passage is because of no cross-pressure gradient along the passage. The horseshoe vortexes only form at the leading edges. The horseshoe vortex near the fifth blade on the pressure side almost dissipates (figure 11(b)), while the horseshoe vortex near the other side is still clearly visible.

Moving from root to tip, the strength of the vortexes adjacent to the suction side decreases further (figure 12(a) and (b)). From figure 12 the horseshoe vortices are recognizable.

The S.S adjacent horseshoe vortex center is located at mid-span while the horseshoe vortex center at the P.S is located in higher spans near the shroud. Also, the horseshoe vortices besides to the suction-side are more intense than the vortices near the pressure side.

According to these contour plots, the velocity in the vortex center is diminishing.

Inflow passage vortex:

Inflow vortex which is caused by the unsymmetrical flow into the radial cascade from the upstream scroll has more intensity in non-flowing sector of rotor than the flowing part in partial case (figure 10 region z). The unsymmetrical inflow forms the inflow vortex. The secondary flow motion is intensified, with accelerating the main flow in the channel which makes the inflow vortex stronger. The vortex center at flowing passages affects much of the flow.

At the entrance of the rotor, inflow vortex can be seen interacting with the horseshoe vortex.

(Figure 10 region a). This interaction is more dominant in non-flowing passages and with the same sense of rotation causes a weakening of the horseshoe vortex. Also, the inflow vortex appears to be the dominant effect in the downstream plane of the rotor. As a rule in the sector with the lower mass flow, the contours change more drastically in contrast with flowing sector leading to the stronger vortex in this region. While with moving to the flowing section the Mach number variations happen smoother with higher Mach number at the core (figure 11(a)).

Surface Mach number of the S.S increases up from leading edge to trailing edge whereas, at the pressure side, it decreases. This phenomenon could be an origin of the formation of inflow passage vortex. This guess could justify by dominating the inflow vortex in passages with the higher mass flow. The results adjust the experimental findings of the Putra and Joos(2013). They find two horseshoe vortexes at the leading edges of the S.s and P.s with decreasing intensity in the stream-wise direction. Also, they recognized a new vortex type called the Inflow vortex in the radial turbine. The presented study is a very beneficial way to adjust their declaration because every passage has a different internal mass flow which shows the formation of the inflow vortex efficiently.

[DOI: 10.22068/ijae.8.4.2817]

Some interaction and dependency between two

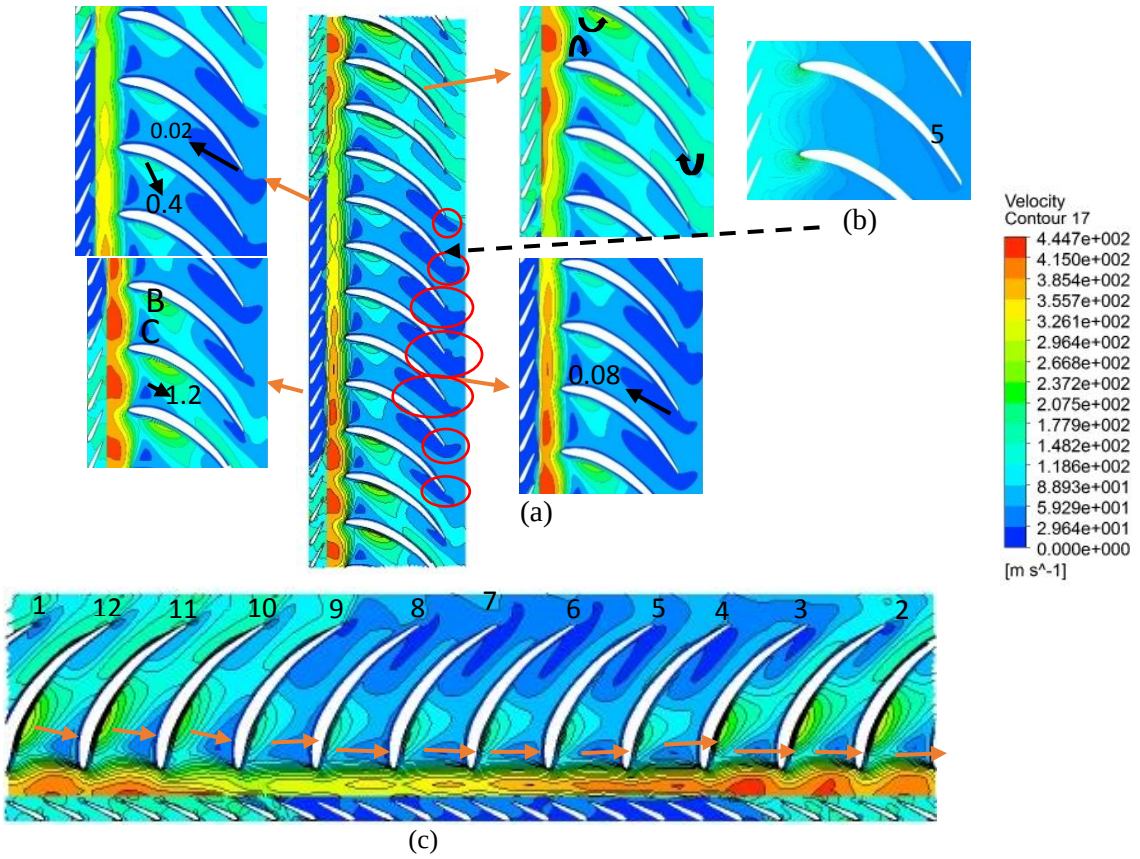

Figure 11. -(a)Mach contour at 50% span of partial condition case,(b) Pressure contour of 5th blade,(c) Velocity contour

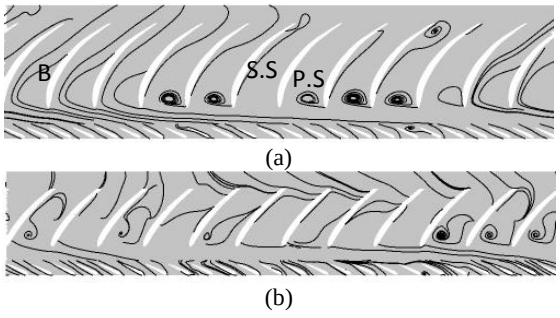

Figure 12. -(a) Stream lines of the partial admission case in 50% span(b) Stream lines of the partial admission case in 80% span

4. CONCLUSIONS

This work increase the knowledge of the flow behavior under different admissions in double entry turbines. Double volute turbocharger turbine under real conditions was investigated:

In partial feeding, efficiency was reduced.

limbs have been recognized in the interspace region. This interaction can be removed by increasing the chord of two stator vanes in tongue region to isolate two sectors completely. It could be investigated in the future study.

Horseshoe vortex, corner vortex, and Inflow vortex generation in passages with different mass inflow was using validated CFD model.

The plots show that the inflow vortex has more intensity in the non-flowing sector of the rotor than the flowing part in the partial case.

Unsymmetrical inlet flow leads to formation of the inflow vortex.

References

[1] Watson N. Janota MS. Turbocharging the Internal Combustion Engines. First ed. London and Basingstoke:The Macmillan Press Ltd;1982.

[2] Sajedin A, Jazayeri SA, ahmadi M, et al. Enhancing The Starting Torque Of Turbocharged SI Engine Using 1-D CFD Simulation. Applied Mechanics and Materials.2012; Vols. 110-116, p 4919-

[DOI: 10.22068/ijae.8.4.2817]

4924.

[3] Chiong MS, Rajoo S, Martinez-Botas R F, et al. Engine Turbocharger Performance Prediction: One-Dimensional Modeling of a Twin Entry Turbine. Energy Conversion and Management. 2012; 57, 68–78.

[4] Copeland CD, Seiler M, and Martinez-Botas R F. Unsteady Performance of a Double Entry Turbocharger Turbine with a Comparison to Steady Flow Conditions. ASME J Turbomach. 2012; 134(2), p. 021022.

[5] Copeland CD, Seiler M, Martinez-Botas RF. Comparison Between Steady and Unsteady Double-Entry Turbine Performance Using the Quasi-Steady Assumption. ASME J Turbomach. 2011; 133(2), p. 031001.

[6] Copeland CD, Newton P, Seiler M, et al. The Effect of Unequal Admission on the Performance and Loss Generation in a Double-Entry Turbocharger Turbine. ASME J. Turbomach.2012; 134(2), p. 021004.

[7] Copeland C. The Evaluation of Steady and Pulsating Flow Performance of a Double-Entry Turbocharger Turbine. Ph.D. thesis, Imperial College of Science Technology and Medicine, University of London, 2010.

[8] Newton P, Copeland C, Martinez-Botas RF, et al. An Audit of Aerodynamic Loss in a Double Entry Turbine under Full and Partial Admission. Int. J. Heat Fluid Flow, 2012; 33, pp. 70–80.

[9] Romagnoli A, Copeland CD, Martinez-Botas RF, et al. Comparison between the Steady Performance of Double-Entry and Twin-Entry Turbocharger Turbines. Proceedings of ASME Turbo Expo 2009; GT2011-45525.

[10] Reising S, Schiffer HP. Non-Axisymmetric End Wall Profiling In Transonic Compressors. Part I: Improving The Static Pressure Recovery At Off-Design Conditions By Sequential Hub And Shroud End Wall Profiling, Proceedings of ASME Turbo Expo 2009; Power for Land, Sea and Air, GT2009.

[11] Fottner L. Review on Turbomachinery Blading Design Problems. AGARD Lecture Series No. 167, 1989.

[12] Ciorciari R. Kirik I, Niehuis R. Effects of Unsteady Wakes on the Secondary Flows in the Linear T106 Turbine Cascade. Journal of Turbomachinery ASME, 2014; Vol. 136 / 091010.

[13] Ghorbanian, K. and Amanifard, N., "A numerical investigation on the unstable flow in a single stage of an axial compressor", International Journal of Engineering-Transactions A: Basics, Vol. 16, No. 2, (2003), 171-180.

[14] Farhanieh, B., Amanifard, N. and Ghorbanian, K., “A Numerical Investigation on the Unstable Flow in a Single Stage of an Axial Compressor”, International Journal of Engineering Transaction A: Basics, Vol. 16, No. 2, June 2003 – 171

[15] Putra MA, Joos F. Investigation of Secondary Flow Behavior in a Radial Turbine Nozzle. Journal of Turbomachinery ASME .2013; Vol. 135 / 061003-1.

[16] Pischinger F, Wunsche A. The Characteristic Behaviour of Radial Turbines and Its Influence on the Turbocharging Process. Proceedings of the 12th International Congress on Combustion Engines, 1977; Tokyo, 545–568.

[17] CFX 14.0 Theory guide in ANSYS 14.0 Help, 2011.

[18] N. Rajabi, R. Rafee, S. Frazam-Alipour “Effect of Blade Design Parameters on Air Flow through an Axial Fan”,International Journal of Engineering TRANSACTIONS A: Basics Vol. 30, No. 10, (October 2017) 1583-1591

[19] Newton P, Romagnoli A, Martinez-Botas RF, et al. A Method of Map Extrapolation for Unequal and Partial Admission in a Double Entry Turbine. Journal of Turbomachinery, ASME, 2014; Vol. 136 / 061019-1.

[20] Binder A, Romey R. Secondary Flow Effects and Mixing of the Wake Behind a Turbine Stator. ASME J. Eng. Power, 1983; 105(1), 4.

[DOI: 10.22068/ijae.8.4.2817]